Biomedical Optics EXPRESS

MEMS-based multiphoton endomicroscope for repetitive imaging of mouse colon

Xiyu Duan,[1] Haijun Li,[2] Zhen Qiu,[1,2] Bishnu P. Joshi,[2] Asha Pant,[2] Arlene Smith,[2] Katsuo Kurabayashi,[3,4] Kenn R. Oldham,[3] and Thomas D. Wang[1,2,3,*]

[1]*Department of Biomedical Engineering, University of Michigan, Ann Arbor, MI, USA*
[2]*Department of Internal Medicine, Division of Gastroenterology, University of Michigan, Ann Arbor, MI, USA*
[3]*Department of Mechanical Engineering, University of Michigan, Ann Arbor, MI, USA*
[4]*Department of Electrical Engineering, University of Michigan, Ann Arbor, MI, USA*
[*]*thomaswa@umich.edu*

Abstract: We demonstrate a handheld multiphoton endomicroscope with 3.4 mm distal diameter that can repetitively image mouse colon in vivo. A 2D resonant MEMS mirror was developed to perform beam scanning in a Lissajous pattern. The instrument has an effective numerical aperture of 0.63, lateral and axial resolution of 2.03 and 9.02 μm, respectively, working distance of 60 μm, and image field-of-view of 300 × 300 μm^2. Hoechst was injected intravenously in mice to stain cell nuclei. We were able to collect histology-like images in vivo at 5 frames/sec, and distinguish between normal and pre-malignant colonic epithelium.

OCIS codes: (170.0170) Medical optics and biotechnology; (060.2350) Fiber optics imaging; (110.0110) Imaging systems; (190.4180) Multiphoton processes; (170.2150) Endoscopic imaging.

References and links

1. W. Denk, J. H. Strickler, and W. W. Webb, "Two-photon laser scanning fluorescence microscopy," Science **248**(4951), 73–76 (1990).
2. A. Masedunskas, M. Sramkova, L. Parente, and R. Weigert, "Intravital Microscopy to Image Membrane Trafficking in Live Rats," Methods Mol. Biol. **931**, 153–167 (2012).
3. M. T. Myaing, D. J. MacDonald, and X. Li, "Fiber-optic scanning two-photon fluorescence endoscope," Opt. Lett. **31**(8), 1076–1078 (2006).
4. C. J. Engelbrecht, R. S. Johnston, E. J. Seibel, and F. Helmchen, "Ultra-compact fiber-optic two-photon microscope for functional fluorescence imaging in vivo," Opt. Express **16**(8), 5556–5564 (2008).
5. Y. Wu, Y. Leng, J. Xi, and X. Li, "Scanning all-fiber-optic endomicroscopy system for 3D nonlinear optical imaging of biological tissues," Opt. Express **17**(10), 7907–7915 (2009).
6. D. R. Rivera, C. M. Brown, D. G. Ouzounov, I. Pavlova, D. Kobat, W. W. Webb, and C. Xu, "Compact and flexible raster scanning multiphoton endoscope capable of imaging unstained tissue," Proc. Natl. Acad. Sci. U.S.A. **108**(43), 17598–17603 (2011).
7. W. Piyawattanametha, R. P. J. Barretto, T. H. Ko, B. A. Flusberg, E. D. Cocker, H. Ra, D. Lee, O. Solgaard, and M. J. Schnitzer, "Fast-scanning two-photon fluorescence imaging based on a microelectromechanical systems two- dimensional scanning mirror," Opt. Lett. **31**(13), 2018–2020 (2006).
8. C. L. Hoy, O. Ferhanoğlu, M. Yildirim, W. Piyawattanametha, H. Ra, O. Solgaard, and A. Ben-Yakar, "Optical design and imaging performance testing of a 9.6-mm diameter femtosecond laser microsurgery probe," Opt. Express **19**(11), 10536–10552 (2011).
9. L. Fu, A. Jain, C. Cranfield, H. Xie, and M. Gu, "Three-dimensional nonlinear optical endoscopy," J. Biomed. Opt. **12**(4), 040501 (2007).
10. K. L. Turner, S. A. Miller, P. G. Hartwell, N. C. MacDonald, S. H. Strogatz, and S. G. Adams, "Five parametric resonances in a microelectromechanical system," Nature **396**(6707), 149–152 (1998).
11. Z. Qiu, Z. Liu, X. Duan, S. Khondee, B. Joshi, M. J. Mandella, K. Oldham, K. Kurabayashi, and T. D. Wang, "Targeted vertical cross-sectional imaging with handheld near-infrared dual axes confocal fluorescence endomicroscope," Biomed. Opt. Express **4**(2), 322–330 (2013).
12. Z. Qiu, S. Khondee, X. Duan, H. Li, M. J. Mandella, B. P. Joshi, Q. Zhou, S. R. Owens, K. Kurabayashi, K. R. Oldham, and T. D. Wang, "Vertical Cross-Sectional Imaging of Colonic Dysplasia In Vivo With Multi-spectral Dual Axes Confocal Endomicroscopy," Gastroenterology **146**(3), 615–617 (2014).

#236523 Received 20 Mar 2015; revised 3 Jul 2015; accepted 21 Jul 2015; published 29 Jul 2015

13. W. Shahid, Z. Qiu, X. Duan, H. Li, T. D. Wang, and K. R. Oldham, "Modeling and Simulation of a Parametrically Resonant Micromirror With Duty-Cycled Excitation," J. Microelectromech. Syst. **23**(6), 1440–1453 (2014).
14. H. Li, Z. Qiu, X. Duan, K. R. Oldham, K. Kurabayashi, and T. D. Wang, "2D resonant microscanner for dual axes confocal fluorescence endomicroscope," in Proceedings of 27th IEEE International Conference on Micro Electro Mechanical Systems (IEEE 2014), pp. 805–808.
15. T. Hinoi, A. Akyol, B. K. Theisen, D. O. Ferguson, J. K. Greenson, B. O. Williams, K. R. Cho, and E. R. Fearon, "Mouse model of colonic adenoma-carcinoma progression based on somatic Apc inactivation," Cancer Res. **67**(20), 9721–9730 (2007).
16. L. Ritsma, S. I. J. Ellenbroek, A. Zomer, H. J. Snippert, F. J. de Sauvage, B. D. Simons, H. Clevers, and J. van Rheenen, "Intestinal crypt homeostasis revealed at single-stem-cell level by in vivo live imaging," Nature **507**(7492), 362–365 (2014).
17. R. Le Harzic, I. Riemann, M. Weinigel, K. König, and B. Messerschmidt, "Rigid and high-numerical-aperture two-photon fluorescence endoscope," Appl. Opt. **48**(18), 3396–3400 (2009).
18. J. C. Jung, A. D. Mehta, E. Aksay, R. Stepnoski, and M. J. Schnitzer, "In vivo mammalian brain imaging using one- and two-photon fluorescence microendoscopy," J. Neurophysiol. **92**(5), 3121–3133 (2004).
19. Y. Wu, J. Xi, M. J. Cobb, and X. Li, "Scanning fiber-optic nonlinear endomicroscopy with miniature aspherical compound lens and multimode fiber collector," Opt. Lett. **34**(7), 953–955 (2009).
20. Y. Zhang, M. L. Akins, K. Murari, J. Xi, M. J. Li, K. Luby-Phelps, M. Mahendroo, and X. Li, "A compact fiber-optic SHG scanning endomicroscope and its application to visualize cervical remodeling during pregnancy," Proc. Natl. Acad. Sci. USA **109**(32), 12878–12883 (2012).
21. D. M. Huland, C. M. Brown, S. S. Howard, D. G. Ouzounov, I. Pavlova, K. Wang, D. R. Rivera, W. W. Webb, and C. Xu, "In vivo imaging of unstained tissues using long gradient index lens multiphoton endoscopic systems," Biomed. Opt. Express **3**(5), 1077–1085 (2012).
22. E. J. Botcherby, C. W. Smith, M. M. Kohl, D. Débarre, M. J. Booth, R. Juškaitis, O. Paulsen, and T. Wilson, "Aberration-free three-dimensional multiphoton imaging of neuronal activity at kHz rates," Proc. Natl. Acad. Sci. USA **109**(8), 2919–2924 (2012).

1. Introduction

Improved imaging methods are needed to visualize the epithelium in genetically-engineered mouse models of human disease. This thin layer of tissue lines hollow organs, such as colon, and is the origin of a number of human cancers. Multiphoton microscopy is a powerful imaging tool for visualizing biological tissues with sub-cellular resolution and provides excellent depth, minimal photodamage, and reduced scattering [1]. Intravital microscopy is an emerging methodology for performing real time imaging in live animals. This technology is playing a greater role in the study of cellular and molecular biology because in vitro systems cannot adequately recapitulate the microenvironment of living tissues and systems. Conventional intravital microscopes use large, bulky objectives that require wide surgical exposure to image internal organs and result in terminal experiments [2]. If these instruments can be reduced sufficiently in size, biological phenomena can be observed in a longitudinal fashion without animal sacrifice.

A fast, compact scanner is needed to perform real time imaging with high performance in a miniature instrument. Previously, multiphoton endomicroscopes based on fiber scanning have been demonstrated [3–6]. This approach can introduce extra off-axis aberrations, and scanning performance is fiber dependent. Alternatively, beam scanning can be performed using tiny mirrors developed with microelectromechanical systems (MEMS) technology. MEMS scanners have been developed previously [7–9], but the overall size of the endomicroscope was not adequately small to perform repetitively imaging in mice. We aim to demonstrate a handheld multiphoton endomicroscope with a small distal diameter of 3.4 mm using a compact high speed MEMS scanner to perform repetitive imaging in the colon of a live mouse with "histology-like" performance. An instrument of this size allows us to capitalize on the many sophisticated mouse models available to study epithelial cancers.

2. Methods

2.1 System architecture

We used a Ti-Sapphire laser (Mai Tai DeepSee HP DS, Spectra-Physics) with a tunable spectral range of 700-1040 nm to deliver excitation (red arrows) with ~100 fs pulse width at

#236523 Received 20 Mar 2015; revised 3 Jul 2015; accepted 21 Jul 2015; published 29 Jul 2015

80 MHz, Fig. 1. The pulse duration was minimized using a dispersion pre-compensation unit located inside the laser housing. A half wave plate (HWP) and linear polarizer (LP) were used in combination to adjust the power. The beam is focused into a 1 meter long hollow core photonic bandgap fiber (PBF) with NA = 0.2 (HC-800-02, NKT Photonics) using a 10X objective lens L_1 with f = 18 mm (RMS 10X, Thorlabs). The PBF fiber transmits light at 780 nm with zero dispersion, thus prechirp was not performed. This fiber can achieve a bend diameter of <1 cm without loss of optical transmission. An aspheric lens L_2 with f = 3 mm (355660-B, Thorlabs) collimates the beam coming out of the fiber to a diameter of 1.2 mm. The beam is reflected by an aluminum (Al) coated mirror M_1 (48-405, Edmund Optics), and passes through a dichroic mirror M_2 (62-634, Edmund Optics) with transmission efficiency >95% at 780 nm onto a custom 2D MEMS scanner M_3 at 45° incidence. The distal optics consists of four miniature lenses L_3-L_6 that focus the excitation beam into the tissue and collect the fluorescence generated. Fluorescence (green arrows) travels in the opposite direction along the same optical path, is descanned by M_3, is reflected by M_2 with reflectivity >90% from 425 to 650 nm, and is focused by lens L_7 with f = 3 mm (355660-B, Thorlabs) into a 1 meter long multimode fiber (MMF) (FT400UMT, Thorlabs) with a large core size of 400 µm to maximize light collection. Fluorescence is collimated by L_8 with f = 15 mm (LA1540-A, Thorlabs), passes through a band pass filter (BPF) (FGB39, Thorlabs) that transmits from 360 to 580 nm with ~80% transmission efficiency, and is focused by lens L_9 with f = 60 mm (LA1134-B, Thorlabs) onto a photomultiplier tube (PMT) detector (H7422-40, Hamamatsu). The PMT signal is amplified by a high-speed current amplifier (59-178, Edmund Optics). Reflectance that passes through M_2 is reflected by M_1 and focused back into the PBF for delivery to a photo diode (PD) detector (2051-FC, Newport).

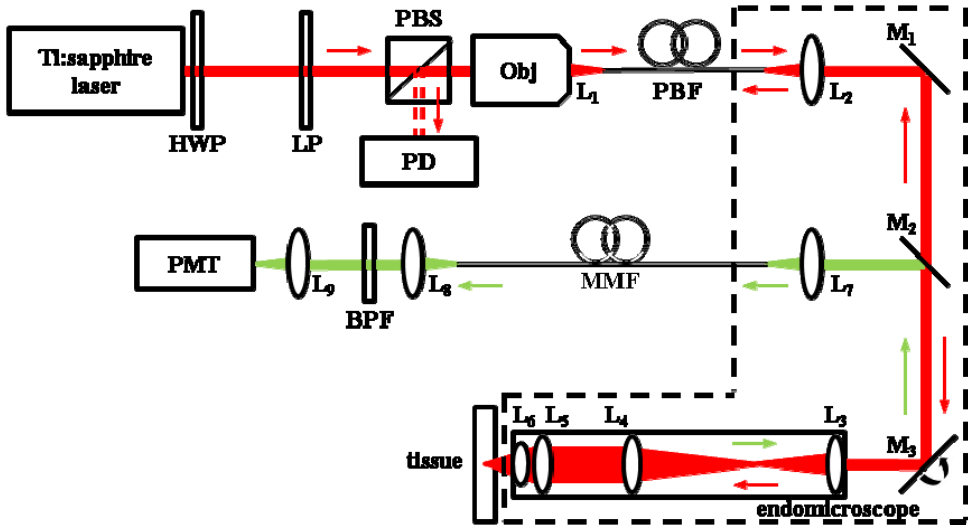

Fig. 1. Schematic. Handheld multiphoton endomicroscope shown in dashed box. Details provided in text.

For laser excitation, the transmission efficiency from the input of the PBF to the output of the endomicroscope at L_6 is ~20%. The PBF has ~50% transmission through the 1 meter length, and the MEMS mirror provides ~70% reflection, which includes a slight overfilling of the mirror and insertion losses from the optics. For fluorescence collection, the transmission efficiency from distal end of the endomicroscope at L_6 back to the PMT is ~50%, resulting from ~70% reflection at the MEMS mirror, ~95% transmission through the multimode fiber (MMF), and ~80% transmission efficiency of the bandpass filter (BPF) before the PMT.

#236523 Received 20 Mar 2015; revised 3 Jul 2015; accepted 21 Jul 2015; published 29 Jul 2015

We used a high-speed multi-function data acquisition board (National Instruments, PCI-6115) to digitize the fluorescence signal from the PMT and the reflectance signal from the photodiode. The same board was used to generate control signals to drive the 2D MEMS scanner. The data acquisition board was controlled by a pc running custom developed Labview programs.

2.2 Optical design

We performed ray-trace simulations (ZEMAX, ver. 13) to identify commercially-available optics to achieve diffraction-limited resolution on axis, Fig. 2. We used achromats for L_3 and L_4 in a telescope configuration to expand the excitation beam to a width of 1.8 mm to fill the back aperture of the focusing optics L_5 and L_6 to maximize the effective numerical aperture (NA) and hence photon flux to generate the fluorescence signal.

2.3 2D MEMS scanner

We developed a 2D MEMS scanner based on the principle of parametric resonance, where large mechanical scan angles can be achieved by driving the structure at $2\omega_0/n$, where ω_0 is the natural frequency of the scanner structure and n is an integer ≥1 [10–13]. The mirror was designed with a 1.8 mm diameter circular reflector to accommodate the 1.2 mm width of the excitation beam at 45° incidence, Fig. 3. When scanning at large mechanical angles up to ± 4.5°, this mirror reflects >95% of the beam. A gimbal frame is used to minimize cross-talk between the X (inner) and Y (outer) axes. Orthogonally oriented inner and outer electrostatic comb-drives actuators are coupled to torsional springs to rotate the mirror about either axis. In this design, the resonant frequencies of the inner and the outer axes were chosen to be ~3 and ~1 kHz, respectively, to image in vivo at ≥5 frame/sec using Lissajous scanning. Custom software was developed in LabView to drive the MEMS scanner and to reconstruct the image by remapping the time series signal to a 2D image using calibrated motion profiles from the scanner to generate a lookup table. The scanner was fabricated using a 3 step deep reactive-ion etch (DRIE) process with 3 masks [14]. Aluminum was sputtered on the front-side silicon surface to improve reflectivity. The mirror curvature and surface roughness were measured using an optical surface profiler (NewView 5000, Zygo).

2.4 Mechanical design and packaging

We used CAD software (Solidworks, ver 2013) to design the housing to package the optics and scanner, Fig. 4. We used an uncoated stainless steel tube with an outer diameter (OD) of 3.4 mm and an inner diameter (ID) of 3 mm to center and align the distal focusing optics. We used Delrin, a non-conductive material with high strength and stiffness, to fabricate the holder. We used copper pins to secure the scanner and to use as contacts for wire bonding the electrical connections. The MEMS scanner and tube were then mounted onto separate 3-axis positioners to align the optics, which was then fixed in place with epoxy (G14250, Thorlabs).

2.5 System resolution

We used 100 nm diameter latex beads (F-8803, Life Technologies) to generate fluorescence for measuring the lateral and axial resolution of the imaging system. These dye-coated microspheres produce peak fluorescence emission at λ_{em} = 515 nm. The lateral resolution was measured from the horizontal fluorescence intensity profile across a single bead in the image, Fig. 5. The axial resolution was determined by scanning the beads in the axial direction using a translational stage. We aimed to achieve an image with a FOV of 300 × 300 μm^2 by sampling with 400 × 400 pixels. To satisfy the Nyquist theorem, we need at least 300 × 300 pixels to sample the FOV with lateral resolution of 2 μm.

#236523 Received 20 Mar 2015; revised 3 Jul 2015; accepted 21 Jul 2015; published 29 Jul 2015

2.6 Imaging of mouse colon

The study was approved by the Michigan University Committee on the Use and Care of Animals (UCUCA). We evaluated n = 5 *CPC;Apc* and n = 5 *Cdx Cre* mice. The *CPC;Apc* mice spontaneously develop colonic polyps in the distal colon that are accessible to the endomicroscope. These mice are genetically engineered to sporadically delete the APC gene, which is mutated in human disease [15]. The *Cdx Cre* mice do not develop polyps, and were used for imaging normal colonic mucosa. During imaging, the mice were anesthetized with inhaled isoflurane. We first used a small animal wide-field endoscope (27030BA, Karl Storz Veterinary Endoscopy) with white light illumination to exam the colon for presence of polyps. For use as landmarks, we measured 1) the distance between the endoscope tip and the anus and 2) the clockwise location of the polyp. Water was delivered through the instrument channel of the endoscope to remove stool, debris, and mucous. Hoechst 33342 (H1399, Life Technologies) at a dose of 10 mg/kg diluted in 200 μL of PBS was delivered intravenously via a tail vein injection to stain the cell nuclei. After 30 min, the distal tip of the endomicroscope was placed in contact with the polyp. Images were collected at 5 frames/sec with a laser power of 50 mW on the mucosa. After completion of imaging, the mice were euthanized. The endomicroscope was oriented perpendicular to the specimen to optimize contact. Images were collected with the same power as that used in vivo. We used the previously identified landmarks to confirm the location of the polyp. The tissues were fixed in 10% buffered formalin and processed for routine histology (H&E). We identified individual frames from the video streams with minimal motion artifacts.

3. Results

3.1 System architecture

The schematic of the imaging system is shown in Fig. 1. Details are provided in Methods, section 2.1.

3.2 Optical design

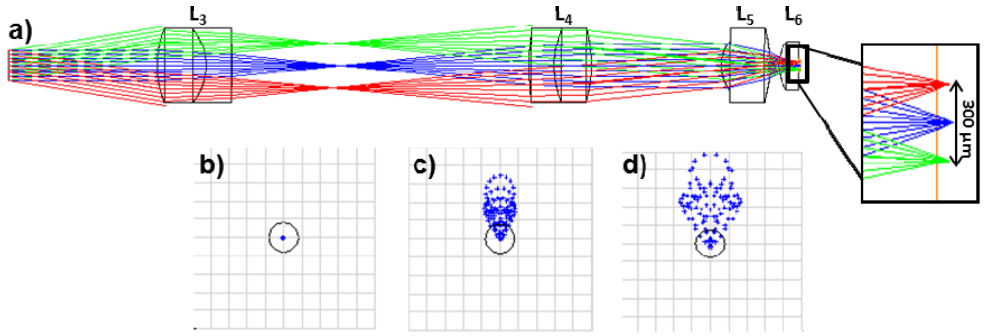

Fig. 2. Zemax Simulation. a) Ray-trace simulation for design of the distal optics (L_3-L_6). A field-of-view (FOV) of 300 × 300 μm^2 can be achieved with a lateral mechanical scan angle of ± 4.5°. b), c), d) Spot size (RMS radius) of 0.33, 1.265 and 2.168 μm can be achieved at a distance of 0, 70 and 150 μm away from the center of the FOV.

Figure 2(a) shows the ray tracing simulation of the optical design using Zemax. We identified commercially-available achromats with OD 3 mm for L_3 with f = 6 mm (45-089, Edmund Optics) and L_4 with f = 9 mm (45-090, Edmund Optics) to produce a telescope configuration. For focusing, we identified an aspheric lens L_5 with OD 3 mm and f = 2 mm (352150-B, Thorlabs) and a plano-convex lens L_6 with OD 2 mm and f = 2 mm (65-265, Edmund Optics). We measured a distance of 0.34 mm between L_5 and L_6 by using a reflectance image to bring a standard USAF target (R3L1S4N, Thorlabs) into focus. This optical configuration has an

#236523 Received 20 Mar 2015; revised 3 Jul 2015; accepted 21 Jul 2015; published 29 Jul 2015

effective NA = 0.63 and a working distance of Z = 60 μm. At this depth, the nuclei in the epithelium of mouse colon can be visualized. We obtained a field-of-view (FOV) of 300 × 300 μm^2 with a lateral mechanical scan angle of ± 4.5°. Zemax simulation results for spot sizes are shown in Fig. 2(b)-2(d). A diffraction-limited spot size with radius R = 0.33 μm was found on the optical axis at X = 0 μm that increased to R = 2.17 μm at X = 150 μm, the lateral extent of the image FOV. With these optics, the frontal focus shifts <30 μm over the wavelength range 450-780 nm used to excite and collect fluorescence. The difference in focus between the excitation and fluorescence wavelengths has little effect on the coupling efficiency of our system because we use a separate, large multi-modal fiber for collection.

3.3 2D MEMS scanner

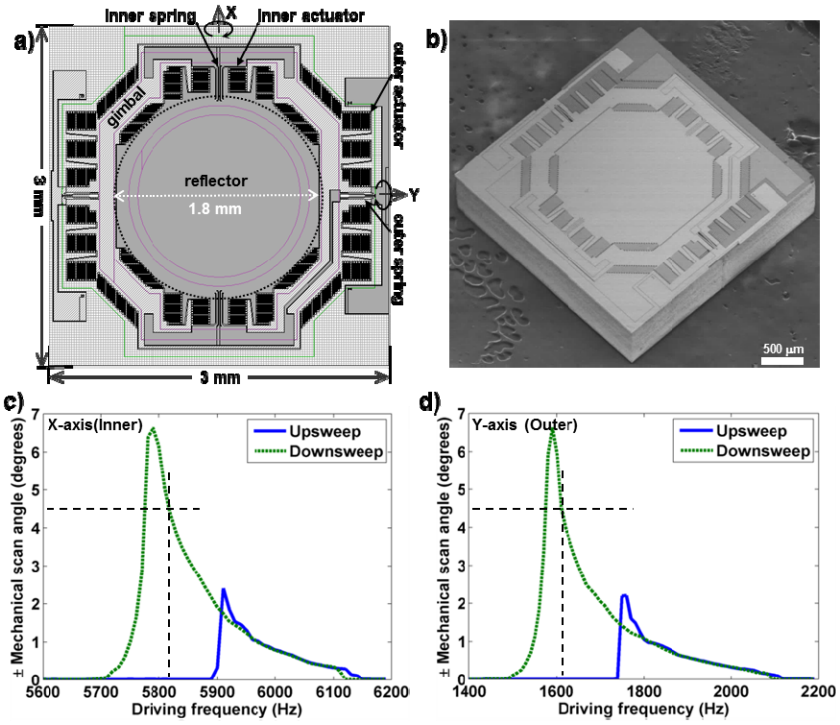

Fig. 3. MEMS scanner. a) Schematic shows dimensions of the 2D MEMS scanner. b) SEM of fabricated scanner. Frequency response for upsweep and downsweep to drive scanner in the c) X and d) Y axes at the fundamental drive frequencies where n = 1.

Figure 3(a) shows a schematic of the 2D MEMS scanner. A 1.8 mm diameter reflector is supported by a gimbal frame on a chip with overall size of 3 × 3 mm^2. The mirror rotates in the XY plane using two orthogonal sets of electrostatic comb-drive actuators. The mirror is coated with a ~50 nm layer of Al. We measured a reflectivity >80% using a 488 and 780 nm, the two key wavelengths used in this study. We did not increase the thickness of the coating because increased stress can deform the reflective surface and change the curvature of the MEMS mirror. The laser is not focused onto the mirror, and we did not observe any mirror damage at the completion of the animal imaging experiments. We found the mirror surface to have a radius of curvature of ~1.7 meter and a root mean square (RMS) roughness of ~2 nm. This result affects the spot size by <10% in the ray trace simulations. Figure 3(b) shows a scanning electron micrograph (SEM) of the fabricated scanner. Figure 3(c) and 3(d) shows the frequency response of the scanner to a sine-wave input at 40 V_{pp} for the X and Y axes, respectively.

#236523 Received 20 Mar 2015; revised 3 Jul 2015; accepted 21 Jul 2015; published 29 Jul 2015

When sweeping from high-to-low frequency in a downsweep (green), we found a larger scan angle compared to sweeping from low-to-high frequency in an upsweep (blue). This phenomenon has been previously demonstrated with parametric resonance scanners [12,13]. This device can achieve ± 4.5° mechanical scan angle at 40 V_{pp} with a drive frequency close to $2\omega_0$ of 5.82 and 1.61 kHz for the X and Y axes, respectively, to produce images at 5 frames/sec with 400x400 pixels to cover a 300 × 300 μm^2 FOV. At larger scan angles, the beam escapes the outer edge of the optics.

Applying these drive frequencies to our parametric resonance scanner, we achieved actual tilting frequencies of 2.91 and 0.805 kHz in the X and Y axes, respectively. This forms a dense Lissajous scan pattern which repeats itself at 5 Hz to encompass images with dimensions of 400x400 pixels with 100% coverage. Since there is a difference in phase between the driving waveform and the actual mirror position, we need to identify the optimal value to best reconstruct the images. We imaged a standard target and manually adjusted the phase with custom Matlab software using a step size of 0.01 degrees until we maximized image resolution.

3.4 Mechanical design and packaging

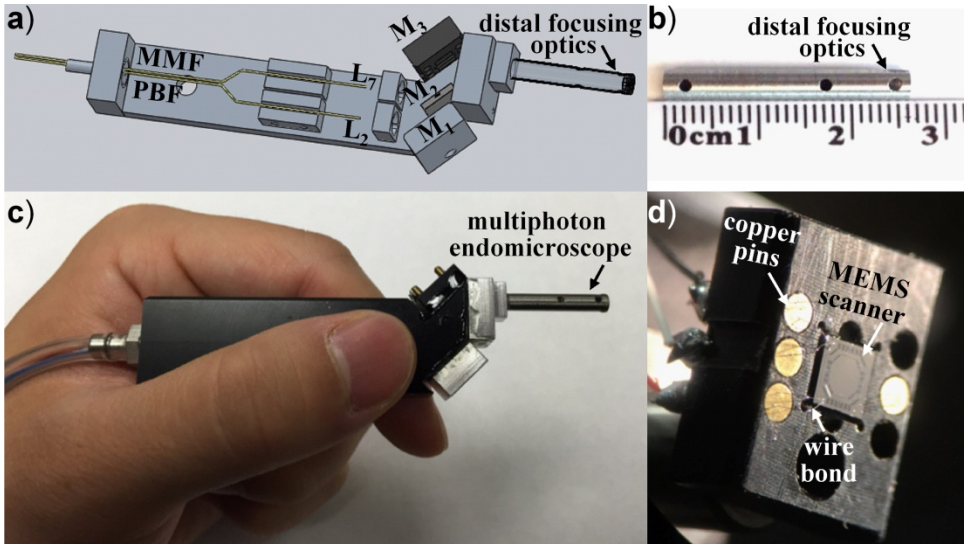

Fig. 4. Endomicroscope packaging. a) CAD drawing. b) Distal focusing optics. c) Handheld instrument can be used to perform repetitive imaging in small animal models of human disease. d) MEMS scanner.

Figure 4(a) shows a CAD drawing of the mechanical package used for the handheld multiphoton endomicroscope. Figure 4(b) shows the stainless steel tube with 3.4 mm diameter and 26 mm length used to align the distal focusing optics. Figure 4(c) shows the instrument held by hand for in vivo imaging. Figure 4(d) shows the custom holder used to house the MEMS scanner M_3.

3.5 System resolution

Figure 5(a) shows a reflectance image of a standard resolution target (USAF 1951) collected with the handheld multiphoton endomicroscope used to adjust the distance between L_5 and L_6. The smallest set of bars (group 7, element 6) can be distinguished (dashed red oval), which represents a dimension of ~2 μm. Figure 5(b) shows a representative fluorescence intensity profile from a 100 nm diameter bead (inset) plotted in the lateral dimension (blue line). The FWHM (full-width at half-maximum) of ΔX = 2.03 μm confirms the lateral

#236523 Received 20 Mar 2015; revised 3 Jul 2015; accepted 21 Jul 2015; published 29 Jul 2015

resolution result. Figure 5(c) shows a representative fluorescence intensity profile of a bead plotted in the axial dimension with FWHM of $\Delta Z = 9.02$ µm.

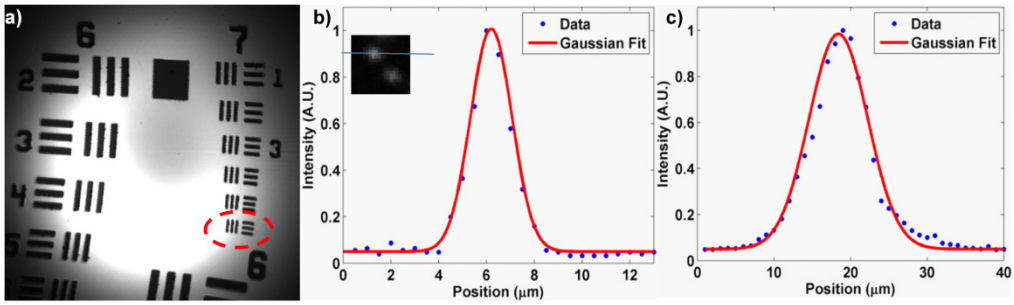

Fig. 5. Image resolution. a) Reflectance image of standard target (USAF 1951). Fluorescence intensity profiles of 100 nm beads show full-width at half maximum (FWHM) of b) 2.03 µm in lateral and c) 9.02 µm in axial directions.

3.6 Imaging of mouse colon

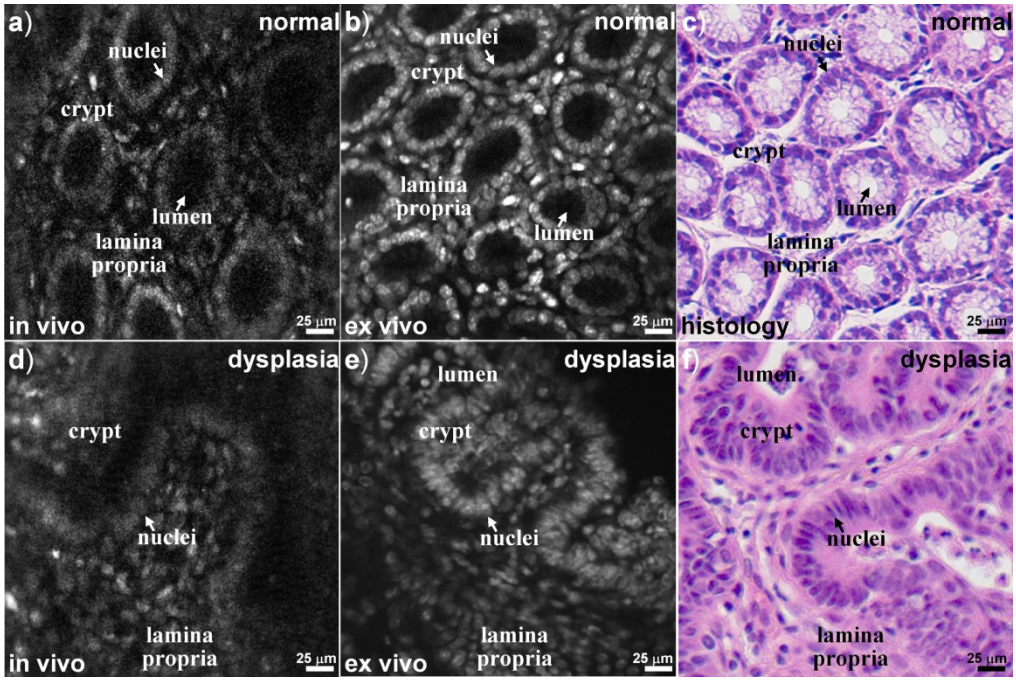

Fig. 6. Imaging results. a) Single frame from multiphoton excited fluorescence video (Visualization 1) of normal colonic mucosa collected in vivo at 5 frames/sec. b) Ex vivo image from normal averaged over 5 frames. c) Corresponding histology (H&E) of normal colon. Single frame from video of dysplastic crypts from colon of *CPC;Apc* mouse collected d) in vivo (Visualization 2) at 5 frames/sec and e) ex vivo (averaged over 5 frames). f) Corresponding histology (H&E) of dysplasia.

We repetitively imaged the colon in live mice three days apart up to five times without any physical signs of trauma, including rectal bleeding, change in activity, and altered behavior. We could identify individual cell nuclei in crypt structures and in the lamina propria. Figure 6(a) shows a representative image of normal mouse colon collected in vivo at 5 frames/sec. The nuclei (arrow) are circular in shape, and the crypts have an oval appearance with similar dimensions and a central lumen (arrow). Figure 6(b) shows these features more clearly on an ex vivo image of normal averaged over 5 frames. Representative histology (H&E) is shown

#236523 Received 20 Mar 2015; revised 3 Jul 2015; accepted 21 Jul 2015; published 29 Jul 2015

for normal, Fig. 6(c). Figure 6(d) shows a representative image of dysplasia from a *CPC;Apc* mouse collected in vivo. The dysplastic nuclei (arrow) appear enlarged and elongated, and the dysplastic crypts are larger in size and distorted in shape. Figure 6(e) shows these features more clearly on an ex vivo image of dysplasia averaged over 5 frames. Histology (H&E) is shown for dysplasia, Fig. 6(f).

4. Discussion

Here, we present a handheld multiphoton endomicroscope with a 3.4 mm distal diameter that can be used to perform repetitive imaging in the colon of genetically-engineered mice. We used a high speed Al-coated MEMS scanner with large mirror surface to maximize the effective NA and photon flux to generate the fluorescence signal. We achieved a mechanical scan angle of ± 4.5 degrees at high frequencies with low drive voltages (<40 V_{pp}) to produce a large FOV of 300 × 300 μm^2 at 5 frames/sec. Decoupling of the tilt motions between the inner and outer axes of the MEMS scanner allows for use of Lissajous scanning at high frame rates. The small distal diameter provides flexibility for use in intravital imaging compared with conventional microscopes that use bulk optics. We found this instrument to have stable operation with minimal interference from mechanical vibrations during in vivo imaging.

Imaging the epithelium of mouse colon with conventional optics and scanners increases experimental complexity and study invasiveness [16]. Surgery is often performed to improve exposure and immobilize organs using custom holders and stages, which can cause bleeding and tissue damage. Coverslips used to flatten and immobilize tissues can cause spherical aberrations. By reducing the distal diameter to 3.4 mm, we achieved "histology-like" images in vivo that could distinguish between pre-malignant and normal colonic mucosa in a mouse model of colorectal cancer. This instrument can be broadly applied to a large number of sophisticated genetically-engineered mouse models of epithelial cancers. A miniature instrument can minimize the number of animals needed, better time the onset of disease, use each animal as its own control, and improve statistical rigor.

Previous multiphoton endomicroscopes have been demonstrated that using miniature scanning technologies. Fu et al reported a 5 mm diameter instrument with 10 μm axial resolution using a 2D mirror based on electrothermal actuation [8]. Fluorescence images were collected ex vivo from rat colon using raster scanning with individual frames collected at 7 lines per sec, a speed that is too slow for in vivo imaging. Hoy et al demonstrated a 10 × 15 × 40 mm^3 handheld instrument with 16.4 μm axial resolution using a 2D MEMS scanner based on electrostatic actuation [7]. Given the large size of this instrument, fluorescence images with a FOV of 310 μm were collected ex vivo from cells embedded in a collagen matrix using Lissajous scanning with individual frames averaged over 5 sec. By comparison, our MEMS scanner has a larger diameter (1.8 mm versus 500 μm) with comparable scan angle, resulting in a >3-fold larger number of resolvable focal spots [7]. Other multi-photon endomicroscopes have used GRIN lenses for focusing [17–20]. These objectives are limited by chromatic aberration for fluorescence imaging [21]. We used a compound lens because our MEMS mirror can achieve high reflectivity over a broad spectral range from 450 to 780 nm.

We used commercially-available lens to demonstrate this approach. Imaging performance can be improved in the future with custom optics. Chromatic aberrations can be reduced to increase fluorescence excitation and collection efficiency. A side rather than front viewing configuration can improve contact with the mucosal surface in hollow organs, such as colon. The MEMS scanner can be designed to perform raster scanning to improve the frame rate and reduce motion artifacts. As a future direction, we are incorporating the MEMS scanner into the distal end of the instrument to increase the length and to adjust the axial imaging depth using a remote fast scanning actuator [22].

#236523 Received 20 Mar 2015; revised 3 Jul 2015; accepted 21 Jul 2015; published 29 Jul 2015

5. Summary

We have developed a novel multiphoton endomicroscope that uses a fast MEMS scanner with 3.4 mm distal optics to perform repetitive in vivo imaging in mouse colon to distinguish between normal and dysplastic crypts. This instrument can be further developed for broad use as a general purpose intravital imaging instrument to perform longitudinal studies in genetically-engineered mouse models of human disease.

Acknowledgments

Funding provided in part by National Institutes of Health U54 CA163059 (TDW), R01 CA142750 (TDW, KK, GDL), U54 CA13642 (TDW), P50 CA93990 (TDW) and S10 RR028819/RR/NCRR (GDL). We thank Steve Donajkowski from the instrument shop for discussion and fabrication of instrument packaging. We thank Gary D. Luker, Zhongyao Liu, Chien-Hung (Coco) Tseng and Prasanth Kalkunte Jayaram for technical support.

#236523 Received 20 Mar 2015; revised 3 Jul 2015; accepted 21 Jul 2015; published 29 Jul 2015